Nanoscale Photoelectron Mapping and Spectroscopy with an Atomic Force Microscope

Ping Yu and Jürgen Kirschner

Max Planck Institute of Microstructure Physics, Weinberg 2, 06120 Halle, Germany

(Received 8 April 2013; revised manuscript received 16 June 2013; published 8 August 2013)

The tip of an atomic force microscope is used as a local probe for photoelectrons excited by laser illumination. The tip-sample distance is precisely controlled by the van der Waals force and the pure photoemission current is measured without tunneling current contribution. The nanoscale photoelectron mapping with high current contrast is obtained on a cesium covered Au(111) surface. By sweeping the laser photon energy, the local photoelectron spectra are measured on Cs islands and terraces. The results reveal distinct electronic states and photoemission thresholds for different Cs coverage, providing the photoemission current contrast mechanism. The contrast in photoelectron mapping can be further tuned by the incident laser polarization exploiting the symmetry selection rules in the optical excitation.

DOI: 10.1103/PhysRevLett.111.067602 PACS numbers: 79.60.Jv, 07.79.Lh, 68.37.Ps

The study of light-matter interaction on the nanometer scale has been boosted by the rapid growth of nanoscience and nanotechnology. In contrast to traditional optical experiments, which investigate the electromagnetic field far away from radiation sources, near-field optical microscopy can identify the local distribution of optical electric field on the nanometer scale [1]. Near-field microscopy is therefore allowed to solve long-standing issues such as the local enhancement of Raman scattering [2] and provide significant insight into the design of optical antenna and plasmonic devices [3]. However, as in all typical optical experiments, detailed information regarding the electronic structure, which plays an important role in the optical excitation, is not directly accessible. This technical barrier can be surmounted by mapping the photoelectrons emitted from the sample surface, which provides information not only of the optical near field [4–6] but also of the local electronic states that contribute to the photoemission (PE) processes [7]. Compared to conventional photoemission electron microscopy, whose spatial resolution is limited by various aberrations, mapping the photoelectrons with the scanning probe microscopy (SPM) technique can offer unprecedented possibilities.

Several groups made significant effort to collect photoelectrons by using the SPM tip as a local detector. Gray and Okuda *et al.* detected the PE current in the tunneling region. To separate the PE current from the tunneling current, they modulated the laser and synchrotron radiation so that the associated modulation of PE current could be measured by a lock-in technique [8,9]. Gimzewski *et al.* detected the PE current by the SPM tip retracted several tens of nm away from the sample surface [10]. Although they obtained submicrometer photoelectron imaging, they did not clarify the origin of the current contrast. So far, there has been no report on the local photoemission spectroscopy measured by the tip in the near-field region, which is a crucial step to investigate the nanometer-scale electron emission properties and understand the contrast mechanism of photoelectron mapping. Here, we report a method to measure the nanoscale photoelectron mapping and spectroscopy in the near-field region by combining atomic force microscopy (AFM) with laser excitation of the tip-sample junction. The tip-sample distance is precisely controlled just beyond the tunneling region while the attractive van der Waals force is still sufficient to stabilize the tip for scanning the surface morphology. With this method, nanoscale PE current mapping with high current contrast is observed on a Cs/Au(111) surface. Different electronic states and photoemission thresholds are observed in the local photoelectron spectra, which contribute crucially to the photoelectron mapping contrast mechanism. Because of the symmetry selection rules in the optical excitation, the PE current mapping contrast depends sensitively on the laser polarization.

The Cs/Au(111) surface is prepared by depositing Cs from a getter source on the Au(111) surface at 300 K. We use the qPlus sensor with a tungsten tip as a local probe which can be operated in either STM or AFM mode [11]. Figure 1(a) shows the STM topography of Cs/Au(111) measured with 0.2 V tip bias and 0.5 nA tunneling current. There are three Cs islands with thickness of 3 monolayer (ML) on top of a 1 ML Cs underlayer. Photoemission can be generated by focusing the laser onto the tip-sample junction. The laser is incident at an angle of 60 deg with respect to the surface normal and focused to 20 μm by a lens in the ultrahigh vacuum chamber with a focal length of 65 mm. The laser has an average power of 1.8 mW with tunable wavelength from 680 to 950 nm [12]. To image the pure PE current, we adjust the frequency shift in the AFM mode for making the tip-sample distance as small as possible but without any tunneling current contribution. This frequency shift is used as a feedback for keeping the tip-sample distance constant while scanning the surface morphology. The PE current flowing within the junction can be detected simultaneously at the sub-pA level using a current-voltage converter [13]. Figures 1(b) and 1(c) are

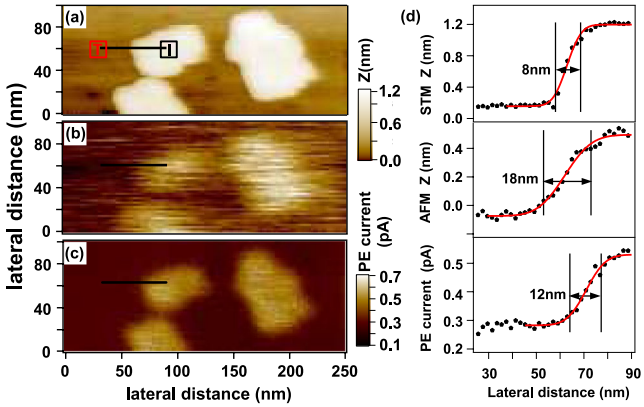

FIG. 1 (color online). (a) Topography image of Cs/Au(111) measured in STM constant current mode ($V_{\mathrm{tip}} = 0.2$ V, $I_{\mathrm{tunnel}} = 0.5$ nA). (b),(c) Topography and PE current images of Cs/Au(111) measured in AFM mode with -1 Hz shift frequency and bias $V_{\mathrm{tip}} = +2$ V. (d) Line profiles crossing the island step edge along the horizontal lines marked in (a)–(c).

the AFM topography and the corresponding PE current images measured at -1 Hz frequency shift and $+2$ V tip bias voltage with 680 nm laser excitation. Without laser illumination, only a constant current background of 150 fA can be detected, which is the leakage current through the electronics. The PE current data shown throughout this Letter are corrected for this dark current background. We find that the PE current values are larger on the Cs islands than on the terrace. The lateral resolution of PE current imaging is estimated by taking line profiles along the horizontal lines as shown in Fig. 1(d). The lateral resolution of 12 nm is obtained from the PE current line profile (16%–84% distance between the minimum and maximum currents). By taking account of 8 nm as the intrinsic width of the island step, which is obtained from the STM line profile, we estimate that the lateral resolution of the PE current imaging is about 4 nm.

To understand the contrast mechanism in the photoelectron mapping, it is important to identify the local work function and electronic states, from which the photoelectrons are optically excited. We measured PE current spectroscopy by sweeping the photon energy in 10 meV steps from 1.33 to 1.83 eV on the Cs island and terrace as marked by I and T in Fig. 1(a), respectively. For each photon energy, the PE current is measured for 50 s and then averaged to the same flux of 6×10^{15} photons per second with p-polarization while the shift frequency and the tip bias voltage are set as -1 Hz and $+2$ V. The averaged PE current values are plotted as a function of the incident photon energy in Fig. 2(a). It clearly shows that the Cs island has a lower photoemission threshold and the PE current is higher than that from the Cs terrace. In Fowler's theoretical model of photoemission, he derived that the quantum yield (number of photoelectrons per incident photon) near the threshold of photoemission is

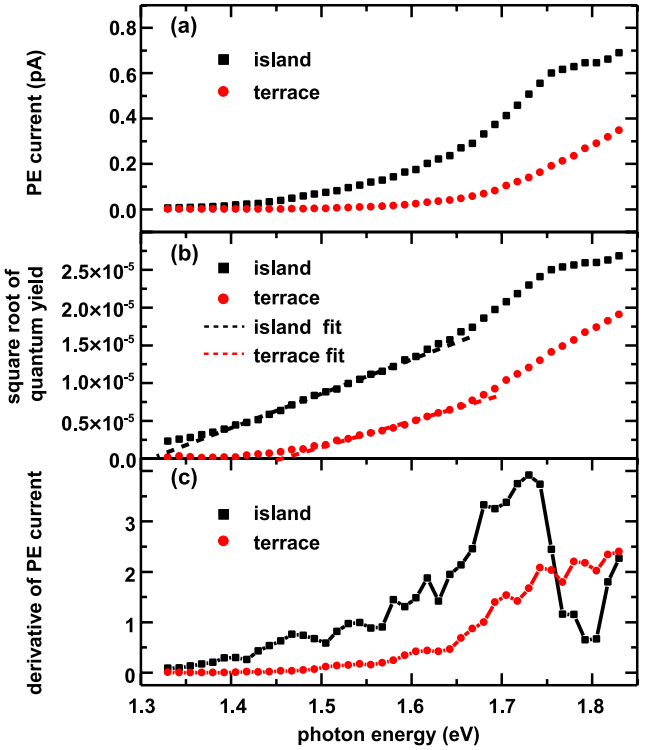

FIG. 2 (color online). (a) Averaged PE current as a function of photon energy measured at the same photon number of 6×10^{15} per second in AFM mode with -1 Hz shift frequency and bias $V_{\mathrm{tip}} = +2$ V on the Cs island and terrace. (b) Square root of quantum yield on the Cs island and terrace are plotted with the photon energy. The dotted lines are the linear fittings near their photoemission thresholds. (c) The derivative of the PE current in (a) with respect to the photon energy for the island and the terrace.

proportional to the square of $h\nu - \varphi$, in which φ is the work function of the sample [14]. By this relation, a plot of the square root of the quantum yield as a function of photon energy should give a straight line intersecting the photon energy axis at the value of the work function. The data points in Fig. 2(b) are the square root of the quantum yield based on the PE current values in Fig. 2(a), and the two dotted lines are the linear fits according to Fowler's model. The values of the work function are determined to be 1.31 and 1.45 eV for the Cs island and terrace. These values are much smaller than the work function of Au(111) (5.31 eV). To explain our observed values of work function, one can first consider the influence of the alkali metal adsorption. Since the Cs ionization potential is less than the Au substrate work function, the valence electrons of Cs adatoms transfer to the substrate which reduces the Au work function to around 2 eV [15,16]. In addition, the work function is reduced by the static electric field between tip and sample. Our tip-sample distance is adjusted just beyond the tunneling region, estimated to be 5 nm [17]. The local barrier for photoelectrons to transport from the sample to the tip can be reduced by the image potential and the

electric field applied by the tip bias, which is about 4×10^6 V/cm in our experiments [18,19]. The photoemission thresholds measured by our method actually represent the local energy barrier at the nanometer tip-sample distance, which can be 0.4 eV lower than the macroscopic work function value in the field of 10^6 V/cm and 5 nm away from the sample surface [20]. Considering these two factors, our observed local energy barriers are reasonable values. We attribute the lower energy barrier on Cs islands to their higher Cs coverage. In previous experiments, it was also observed that the work function of Na overlayers on Cu(111) reaches its maximum value at one monolayer and then drops down by about 0.2 eV when the second layer is formed [21]. The work function of alkali metal films as a function of thickness was also investigated. For Cs, it has been found that its work function gets maximum value at 1.5 monolayer, and is reduced at higher thicknesses [22]. Thus, the thickness dependence is one possible reason for Cs islands showing higher photoemission current and lower threshold than the Cs terrace.

In addition to the local energy barrier difference between Cs islands and terraces, their contributing electronic states in the photoemission process are different. Figure 2(c) shows the derivative photoelectron spectra by differentiating the PE current in Fig. 2(a) with respect to the photon energy $h\nu$. In a simple approximation, the derivative photoelectron spectrum represents the joint density of states involved in the photoemission process [23]. As seen in Fig. 2(a), the derivative photoelectron spectrum on the Cs island shows a pronounced peak at photon energy of about 1.7 eV while the spectrum on the terrace shows a monotonic increase with photon energy without any peak feature. Since only electrons at the Fermi level can be excited at the threshold photon energy, the peak at 1.7 eV observed on the Cs island ($\varphi = 1.3$ eV) indicates an electronic state at 0.4 eV below the Fermi level probed by photoemission. Although there has been no report on the electronic structure of Cs/Au(111), we can take Cs/Cu(111) as a reference since Au(111) and Cu(111) have quite similar electronic band structures. They both possess an sp-band gap along the [111] direction and within the gap there is a surface state located below the Fermi level [24]. Lindgren and Walldén found that the Cu(111) surface state shifts to lower energy with increasing Cs coverage. After 0.5 ML of Cs adsorption, the Cu(111) surface state reaches the lower edge of the gap and then disappears [25]. Because of the band gap of the substrate, the valence electrons in the Cs overlayer are reflected between the substrate and the vacuum interface. Quantum well states are observed in multilayers of Cs on Cu(111) [26]. For 4 ML Cs coverage, the quantum well state is observed at 0.39 eV below the Fermi level [27]. Based on the results of Cs/Cu(111), we infer that the electronic state in our derivative spectrum on the Cs island could originate from the quantum well state of Cs valence electrons confined by the Au(111) band gap and the vacuum interface. Moreover, in our experiments, the Cs islands have the same height. Increasing the Cs coverage leads to the increase of island number and lateral size rather than the island height. At higher Cs coverage, Cs atoms form amorphous clusters instead of well-ordered islands. This preferred height of Cs islands might be connected to the quantum well state, in which, if the energy contribution of the quantized electronic state in the Cs overlayers prevails over the strain energy, a particular height is energetically more favorable than others [28].

We have changed the polarization of the exciting laser field to provide insight into the symmetry properties of the Cs induced electronic states involved in the photoemission process. Figure 3(a) shows the optical geometry for p- and s-polarized excitation in our experiments. The shaded area displays the optical plane spanned by the incident laser beam and the surface normal. The polarization rotation

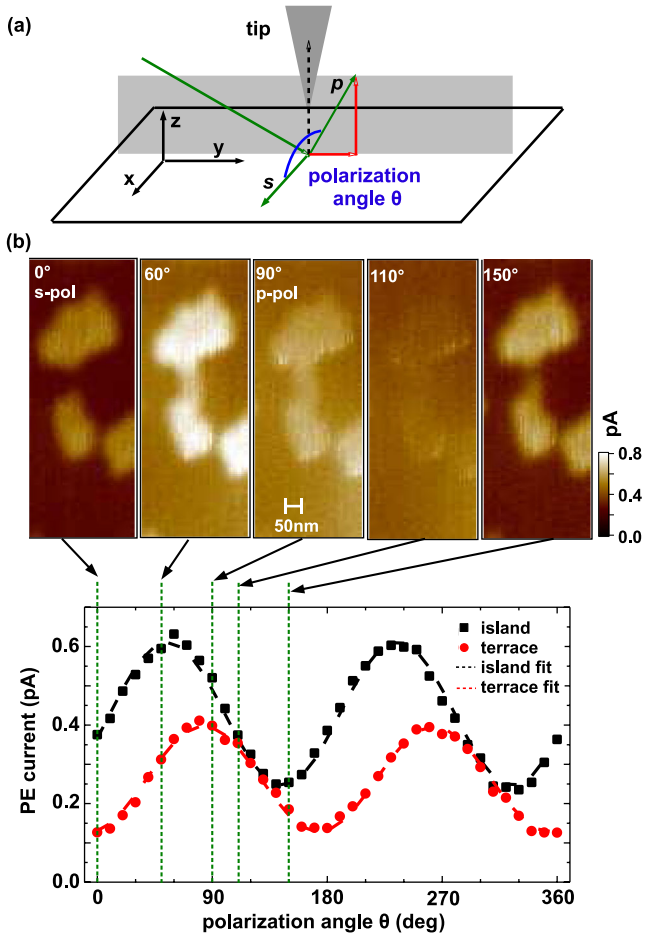

FIG. 3 (color online). (a) Optical geometry for p- and s-polarized excitation. (b) The PE current as a function of the polarization rotation angle on Cs island and terrace. The dotted lines are fittings with the square of the electric field: $a\cos\Theta\hat{e}_x + b\sin\Theta\sin30°\hat{e}_y + c\sin\Theta\cos30°\hat{e}_z$. For Cs island $a = 3.5 \times 10^{-7}$, $b = 4.9 \times 10^{-7}$, $c = 2.9 \times 10^{-7}$, while for terrace $a = 5.9 \times 10^{-8}$, $b = 5.1 \times 10^{-7}$, $c = 3.0 \times 10^{-7}$.

angle θ is defined as the angle between s-polarization and the adjusted polarization. The x, y, and z axes represent the $[1\bar{1}0]$, $[11\bar{2}]$, and [111] directions (along the tip) of Au(111) substrate. With p-polarization, the optical electric field not only has its perpendicular vector along the tip but also has an in-plane component along the crystal direction $[11\bar{2}]$. The optical electric field can be calculated by projecting it onto the x, y, and z directions. Figure 3(b) shows the PE current as a function of the polarization angle on a Cs island and the terrace, respectively. The data points are measured with -1 Hz shift frequency and $+2$ V tip bias voltage with 680 nm laser illumination. The laser polarization is rotated from s-polarization in 10 deg steps to 360 deg. The main difference between the Cs island and the terrace is that the PE current on the terrace gets its highest value with p- polarization while for the Cs island the PE current maximum is at 36 deg away from p-polarization. According to the golden rule formula, the PE current is proportional to the square of matrix elements of the dipole operator with the initial and final state [29]. We fit the experimental data of PE currents with the square of the optical electric field $a\cos\Theta\hat{e}_x + b\sin\Theta\sin30^\circ\hat{e}_y + c\sin\Theta\cos30^\circ\hat{e}_z$. The fitting parameters represent the photoemission transition dipole moments along the different optical electric field directions (x, y, and z). Comparing the fitting parameters of Cs island and terrace, we find that their photoemission transition dipole moments along the y and z directions of the optical electric field are nearly the same. The main difference is the value of the transition dipole moment along the x direction of the optical electric field, in which the dipole moment of the Cs island is 1 order of magnitude larger than that of the Cs terrace. Thus, it is the in-plane electric field orientation which makes the difference, suggesting that the electronic states on the Cs island and terrace have different in-plane orbital symmetries. According to the selection rule, since the final state of normal emission is symmetric with respect to reflection about the optical plane, for the optical electric field along the x direction, normal to the optical plane, only an odd initial state such as p-type orbital oriented along the x direction (p_x) can lead to a photoemission signal [30]. So we infer that, compared to the Cs terrace, Cs islands have an additional p_x orbital symmetry. As a consequence, Cs islands and terraces get maximum PE currents at different laser polarizations. Thus, the contrast of PE current mapping depends on the laser polarization, as shown in Fig. 4. The current contrast (difference divided by the sum) between the Cs island and terrace is plotted as a function of the polarization angle, which shows a maximum contrast at about 20 deg and a minimum contrast at about 110 deg. The dotted curve in Fig. 4 is a fit with the square of the difference between the x and y components of the electric field $(a\cos\Theta\hat{e}_x - b\sin\Theta\sin30^\circ\hat{e}_y)$, agreeing qualitatively with the experimental data. This confirms our inference that, due to the different in-plane orbital symmetries, the PE current contrast depends on the variation of the in-plane electric field.

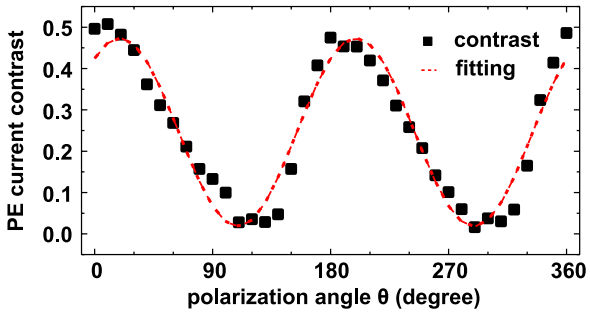

FIG. 4 (color online). Polarization dependence of PE current imaging contrast between Cs islands and terraces. The dotted line is a fitting of the square of the difference between the x and y components of the electric field.

Using our method, we successfully probed the local orbital character of the Cs state and separated the p_x and p_y orbital contributions. We found that the p_y orbital dominates the photoemission process on the Cs terrace. While on the Cs islands, there is an additional p_x orbital symmetry besides the p_y orbital symmetry. The increase of the p_x orbital contribution on the Cs islands can be understood in a simple physical picture: the x direction is along the $[1\bar{1}0]$ crystal direction of the Au(111) substrate, which is the shortest bonding direction for the fcc(111) surface. Thus, the in-plane electronic orbital overlap of the substrate is much stronger along the x direction than that along the y direction. On the Cs terrace, which has only one Cs layer, the hybridization of the p_x orbital between the Cs layer and the substrate must be stronger than that of the p_y orbital. Thus, the Cs state with p_x orbital symmetry cannot be confined between the vacuum level and the substrate band gap on the Cs terrace. On the Cs islands, due to the Cs thickness increase, the hybridization of the electronic states between the Cs layer and the substrate gets much weaker. The electronic states with p_x and p_y orbital symmetries are both well confined between the substrate band gap and the vacuum barrier. This picture is also consistent with our photoelectron spectrum result that a peak feature of the electronic state is observed only on the Cs island, which we attribute to the Cs quantum well state.

To summarize, near-field photoemission current mapping with nanometer resolution is obtained by illuminating the junction with the laser while the tip-sample distance is set precisely beyond the tunneling region. Different electronic states and photoemission thresholds are observed on Cs islands and terraces by measuring the local photoelectron spectra, which crucially contribute to the contrast mechanism of the photoelectron mapping. By adjusting the laser polarization, it is found that the initial state of the Cs island has an additional p-type orbital along the $[1\bar{1}0]$ direction, which leads to the laser polarization dependent PE current mapping contrast. This method can be

widely used to investigate the electronic state and orbital symmetry of nanostructured materials under optical excitation and to explore the mechanism of near-field photoemission.

We acknowledge helpful discussions with C.-T. Chiang.

[1] D. K. Gramotnev and S. I. Bozhevolnyi, Nat. Photonics **4**, 83 (2010).

[2] B. Pettinger, B. Ren, G. Picardi, R. Schuster, and G. Ertl, Phys. Rev. Lett. **92**, 096101 (2004).

[3] L. Novotny and N. V. Hulst, Nat. Photonics **5**, 83 (2011).

[4] J. Lehmann, M. Merschdorf, W. Pfeiffer, A. Thon, S. Voll, and G. Gerber, Phys. Rev. Lett. **85**, 2921 (2000).

[5] A. Kubo, K. Onda, H. Petek, Z. J. Sun, Y. S. Jung, and H. K. Kim, Nano Lett. **5**, 1123 (2005).

[6] M. Cinchetti, A. Gloskovskii, S. A. Nepjiko, G. Schönhense, H. Rochholz, and M. Kreiter, Phys. Rev. Lett. **95**, 047601 (2005).

[7] D. Thien, P. Kury, M. Horn-von Hoegen, F.-J. Meyer zu Heringdorf, J. van Heys, M. Lindenblatt, and E. Pehlke, Phys. Rev. Lett. **99**, 196102 (2007).

[8] S. M. Gray, J. Electron Spectrosc. Relat. Phenom. **109**, 183 (2000).

[9] T. Okuda, T. Eguchi, K. Akiyama, A. Harasawa, T. Kinoshita, Y. Hasegawa, M. Kawamori, Y. Haruyama, and S. Matsui, Phys. Rev. Lett. **102**, 105503 (2009).

[10] J. K. Gimzewski, R. Berndt, and R. R. Schlittler, Ultramicroscopy **42–44**, 366 (1992).

[11] F. J. Giessibl, Appl. Phys. Lett. **76**, 1470 (2000).

[12] Fianium ultrafast fiber laser SC400-PP-AOTF, Fianium Ltd. Unit 20 Compass Point, Hamble, Southampton, UK.

[13] VT SPM, Omicron Nanotechnology GmbH, Germany.

[14] R. H. Fowler, Phys. Rev. **38**, 45 (1931).

[15] N. D. Lang, Phys. Rev. B **4**, 4234 (1971).

[16] G. S. Leatherman and R. D. Diehl, Phys. Rev. B **53**, 4939 (1996).

[17] R. G. Lerner and G. L. Trigg, *Encyclopedia of Physics* (Wiley-VCH, New York, 1991), 2nd ed., p. 1308.

[18] E. O. Lawrence and L. B. Linford, Phys. Rev. **36**, 482 (1930).

[19] W. S. Huxford, Phys. Rev. **38**, 379 (1931).

[20] E. Guth and C. J. Mullin, Phys. Rev. **59**, 867 (1941).

[21] D. Tang, D. McIlroy, X. Shi, C. Su, and D. Heskett, Surf. Sci. Lett. **255**, L497 (1991).

[22] J. J. Brady, Phys. Rev. **41**, 613 (1932).

[23] S. Miyazaki, M. Narasaki, M. Ogasawara, and M. Hirose, Solid State Electron. **46**, 1679 (2002).

[24] S. D. Kevan and R. H. Gaylord, Phys. Rev. B **36**, 5809 (1987).

[25] M. Breitholtz, V. Chis, B. Hellsing, S.-Å. Lindgren, and L. Walldén, Phys. Rev. B **75**, 155403 (2007).

[26] S.-Å. Lindgren and L. Walldén, in *Electronic Structure*, edited by S. Holloway, N. V. Richardson, K. Horn, and M. Scheffler, Handbook of Surface Science Vol. 2 (Elsevier Science, Amsterdam, 2000).

[27] S.-Å. Lindgren and L. Walldén, Phys. Rev. Lett. **61**, 2894 (1988).

[28] L. Gavioli, K. R. Kimberlin, M. C. Tringides, J. F. Wendelken, and Z. Y. Zhang, Phys. Rev. Lett. **82**, 129 (1999).

[29] *Solid-State Photoemission and Related Methods*, edited by W. Schattke and M. van Hove (Wiley-VCH, New York, 2003).

[30] H. Lüth, *Solid Surfaces, Interfaces and Thin Films* (Sprnger, Heidelberg, 2010), 5th ed.